

Centrifuged experiments of continental scale tectonics in Asia

GILLES PELTZER

Peltzer, G. 1988 12 30: Centrifuged Experiments of continental scale tectonics in Asia. *Bulletin of the Geological Institutions of the University of Uppsala*, N.S., Vol. 14, pp. 115–128, Uppsala. ISSN 0302-2749.

Large scale collisional tectonics in Asia are studied with unilaterally confined indentation experiments on 3-D scaled models. The analog material used for the continental lithosphere has a strain-softening behaviour and deforms by faulting. A correct dynamical scaling of the two-layer model with respect to gravity is achieved in a centrifuge at 80g. The experiment shows that: (1) the total shortening of the upper layer is accommodated both by thickening ($\approx 30\%$) and by lateral extrusion of blocks ($\approx 70\%$) guided by large strike-slip faults. (2) Most of the thickening is concentrated in a triangular zone in front of the indenter. (3) Rifts form along strike-slip faults near the free edge of the model. The results are compared with those obtained in 2-D on plasticine models. The geographical distribution of thickened zones and regions of rifting in Asia correspond well with inferences derived from the experiments.

G. Peltzer, Laboratoire de Tectonique, Institut de Physique du Globe de Paris, 4 Place Jussieu, 75252 PARIS Cedex 05, France. Now at: Jet Propulsion Laboratory, California Institute of Technology, 4800 Oak Grove Drive, Pasadena, CAL. 91109, USA. Received 6th June 1987, revision received 20th December 1987.

Introduction

Among the various approaches applied to the problem of continental collision, deformation experiments on analog materials have been shown to be well adapted (Peltzer et al., 1982; Tapponnier et al., 1982). The main reason for this success is due to the fact that, within continents, deformation is often localized into narrow shear zones at the scale of the lithosphere and large strains produce progressive patterns of deformation involving complex fault geometries and kinematics. By contrast with other methods such as analytical and numerical techniques (Villotte et al., 1982; England and McKenzie, 1982), localization of the strain and formation of faults is easily accessible to deformation experiments performed on common plastic materials such as plasticine, clay, sand or other kinds of powder based material (e.g. Caquot and Kerisel, 1949; Peltzer, 1983; Peltzer et al., 1984; Davy, 1987).

In Asia (Fig. 1) the 2 000 to 3 000 km of total shortening induced by the collision with India has produced patterns of deformation in which thickening and thrust faulting are associated with large strike-slip faults (Molnar and Tapponnier, 1975; Tapponnier and Molnar, 1976, 1977). In a first approach to this problem, we performed a series of laboratory experiments in which a plasticine block was indented by a rigid die under plane-strain conditions (Peltzer et al., 1982; Tapponnier et al., 1982;

Peltzer, 1983; Peltzer and Tapponnier, in press). The aim of this study was to analyse the growth and evolution of strike-slip faults in a 2-D deformation under asymmetric boundary conditions (Fig. 2). We then proposed a model for Cenozoic tectonics in Eastern Asia involving the successive eastward extrusion of two large continental blocks (B_1 : Sundaland and B_2 : China, Fig. 1) along two major left-lateral strike-slip faults (respectively the Red River and the Altyn Tagh faults; Peltzer et al., 1982; Tapponnier et al., 1982). Though the geology of E Asia appears to corroborate most of the inferences derived from the plasticine experiments, this simple 2-D approach has been criticised for a variety of reasons. It is clear that the most serious shortcoming with this approach is the plane-strain restriction which prevents any thickening and makes the experiments unscaled with respect to gravity.

We had therefore to address two questions: (1) Is plane-strain a necessary condition to produce strike-slip faulting and horizontal extrusion such as we observed in the plasticine experiments? (2) If both plane-strain and thickening occur simultaneously during indentation, what fraction of the total shortening is accommodated by each of these two competitive processes?

As a step forward in the experimental field, we present here a three dimensional indentation experiment carried out in a centrifuge in order to achieve correct scaling with respect to gravity

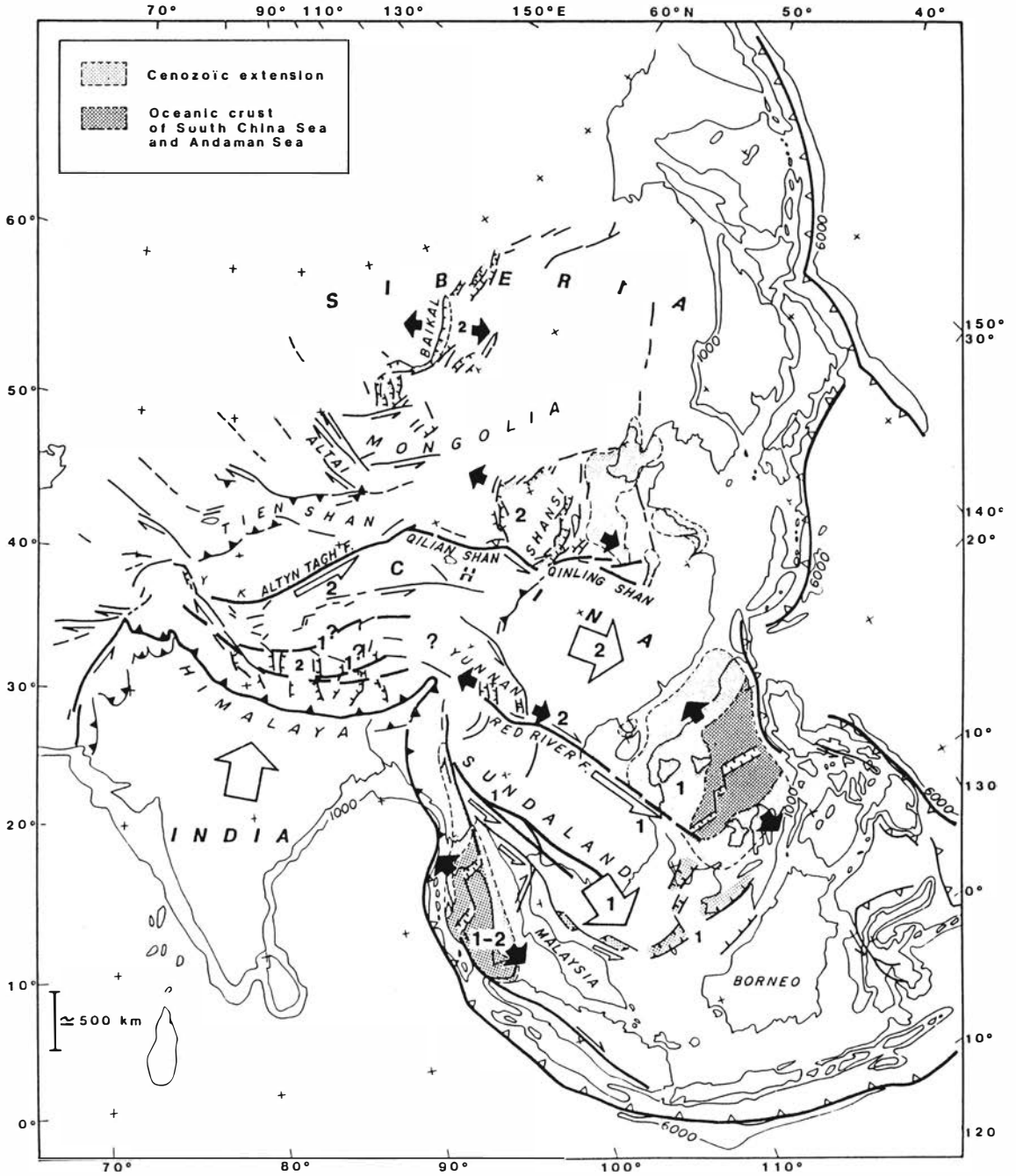
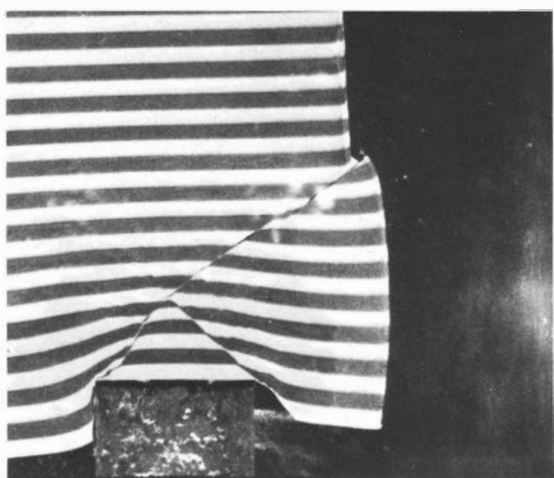
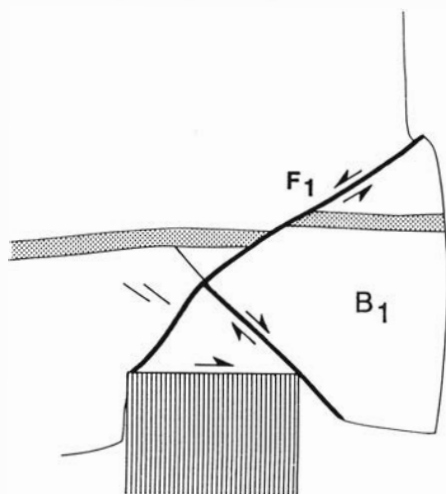


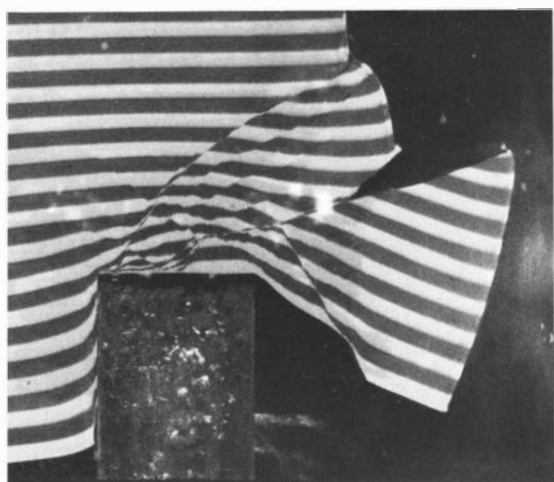
Fig. 1. Schematic map of Cenozoic 2-phase extrusion tectonics in Asia. Heavy lines: major faults or plate boundaries; thin lines: less important faults. Open bars indicate subduction; solid bars, intra-continental thrusts. White arrows represent qualitatively major block motions with respect to Siberia. Black arrows indicate direction of extrusion-related extension. Numbers refer to extrusion phases: 1 ≈ 50 to 20 Ma; 2 ≈ 20 to 0 Ma. Arrows on faults in SW Sundaland, Gulf of Thailand and SW China Sea correspond with Middle Tertiary movements and not present day movements (modified from Tapponnier et al., 1986).



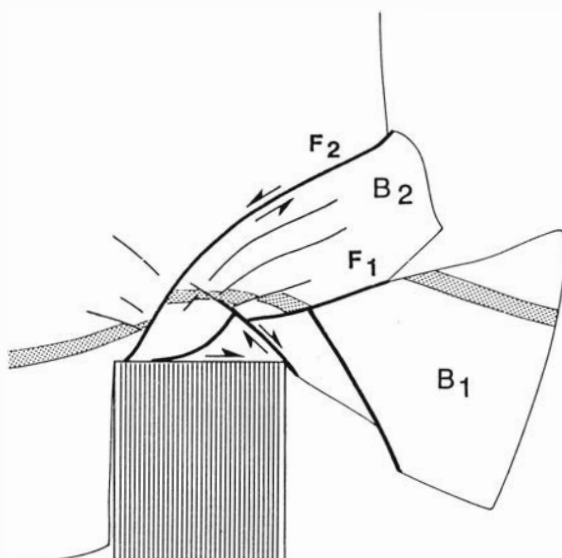
a



c



b



d

Fig. 2. *a and b.* Plane-strain indentation experiment on a layered plasticine block with free boundary on right-hand side, initially 2.5 cm away from the right tip of the indenter. Penetration of the indenter is 2 cm in (a) and 6 cm in (b).
c and d. Geometry of faulting at stages of Figures 2a and 2b involving the successive extrusion and rotation of two blocks B₁ and B₂ (after Peltzer, 1983).

stresses. Our first plasticine models showed the paramount influence on the deformation of the free lateral boundary along the Eastern margin of the Asian continent where oceanic subduction occurs. We have imposed here similar asymmetric boundary conditions. We have thus compared 3-D deformation patterns caused by asymmetric indentation with those of the 2-D case.

From photographs taken during the rotation of the centrifuge, we analyze surface deformations at different stages of the experiment and quantify the balance of deformation in terms of thickening versus plane horizontal strain. We finally discuss these results and compare them with the Tertiary geology of Eastern Asia.

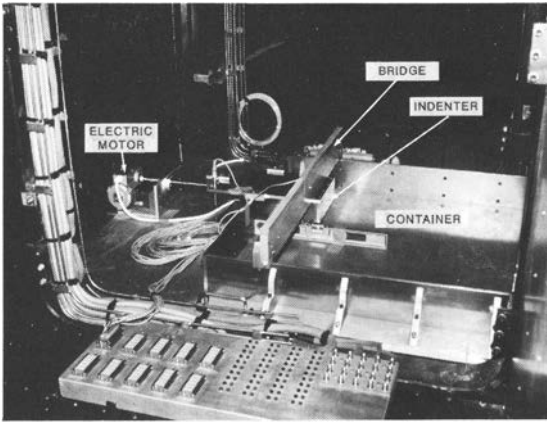


Fig. 3. Experimental device placed in the centrifuge basket. Indenter is coupled with a screw-jack and maintained by a rigid bridge rolling on the two sides of the container in order to resist centrifuge acceleration. Screw-jack is pushed by a speed controlled electric motor.

Experimental set up

Experimental device

The Acutronic centrifuge of the Laboratoire Central des Ponts et Chaussées in Nantes (France) has been designed principally for geotechnical purposes. The payload is 2 tons at centrifugal accelerations up to 100 g, and 500 kg up to 200 g. The size of the basket platform is 1.4 m×1.15 m and the available height is 1.5 m. During the run up time, the swinging basket of the centrifuge progressively rotates about a horizontal axis so as to remain always perpendicular to the resultant of the body forces (centrifugal + gravity forces). In its final position, the platform of the basket lies 5.5 m away from the rotation axis. This large radius implies that the centrifugal force gradient is negligible within most models of small thickness.

The experimental set up is composed of a 90 cm × 80 cm × 11 cm container, and a rigid 20 cm-wide indenter whose linear displacement is guided by a strong bridge rolling on the two lateral sides of the container in order to resist centrifugal forces (Fig. 3). The indenter is moved at a constant velocity by means of a screw-jack coupled to a speed-controlled electric motor. During the experiment, the advance of the indenter is measured at any stage by a displacement captor. The recording of surface deformations (in map view) is achieved by a camera taking photographs at regular intervals. In order to reduce the centrifugal forces applied to the camera, it was set in the arm of the centrifuge about half way from the rotation axis. In addition to this, a video

camera provided continuous monitoring of the whole device.

Geometry of the experiments and boundary conditions

The geometry of the experiment, in the horizontal plane and in a vertical cross section, is shown on Figure 4. The model is made of two different parts: a thin rectangular block of material 1 (continental lithosphere) floats on a denser fluid of material 2 which compensates isostatically the thickening or stretching of the floating block. A rigid indenter moving horizontally at the constant velocity of 2.5 cm/min is pushed into the single layer floating block. At the end of the experiment, the total displacement of the indenter is 20 cm (i.e. a distance equal to its width). As in the 2-D plasticine experiments (Fig. 2), the floating block is set so that its left-hand and far sides touch the walls of the container. Stresses corresponding to the isostatic pressure exerted by material 2 on material 1 are the only ones to act on the right-hand side of the block. During the run-up phase of the centrifuge, the two layer model progressively deforms as its upper free

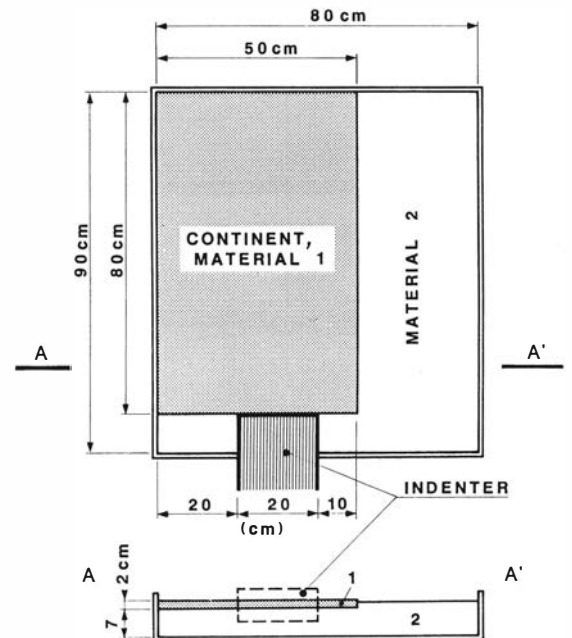


Fig. 4. Map and EW cross-section views of experiment geometry. Single layer model of material 1 floats on denser material 2. Lateral boundary conditions are similar to those in plasticine experiment of Figure 2: the right-hand side boundary is free (only isostatic stress is applied by material 2) and initially lay at a distance from the right tip of indenter equal to half of its width.

surface adjusts to the cylindrical equipotential surface of the radial acceleration field. In the final position of the centrifuge basket, the generating lines of that surface are parallel to the lateral free side of the model. Given the 5.5 m radius of the centrifuge, this implies that the 50 cm wide block is bent by a total angle of 5.2° . We have observed that such a small deformation induces negligible effects on the strains and fault patterns caused by indentation.

Another problem we encountered during the run-up phase was a small shift of the floating block away from the left-hand side wall of the container. This shift may be due to the tangential component of acceleration induced by the speeding up of the centrifuge. Consequently, at the beginning of the experiment, the model is unconfined on both right and left sides, until the deformation caused by the indenter pushes its left-hand side back in contact with the wall of the container. The influence of this unforeseen departure from the initial boundary conditions on the pattern of deformation is discussed in a later section.

Rheology of materials

Material 1:

The first material (continent) is a mixture of 80–150 μm microballs of bronze, microballs of glass of the same diameter range, and silicone oil. The relative mass fraction of bronze and glass microballs allows us to adjust the correct density and silicone oil is added to give a slight cohesion to the mixture. In the present experiment we have chosen mass fractions of 56 % of bronze, 44 % of glass and 68 g/kg of oil so that material 1 has a density $\rho = 2.8 \text{ g/cm}^3$. Compression tests have shown that material 1 has a strain softening behavior for a bulk strain of about 10 % and for greater strains, deformation concentrates into narrow faults. Triaxial tests and vane tests have revealed a Coulomb behavior with a low friction angle of 19° and a cohesion of 2 to 2.5 kPa (Figs. 5 a and b).

Material 2

The second material (asthenosphere) is composed of a homogeneous mixture of clay, a fine lead powder, and the same silicone oil as that used in material 1. The role of clay in this mixture is to keep lead particles in suspension in the viscous fluid. A density of 3.3 g/cm^3 was obtained with the following mass fractions: 82 % of lead, 18 % of clay and 210

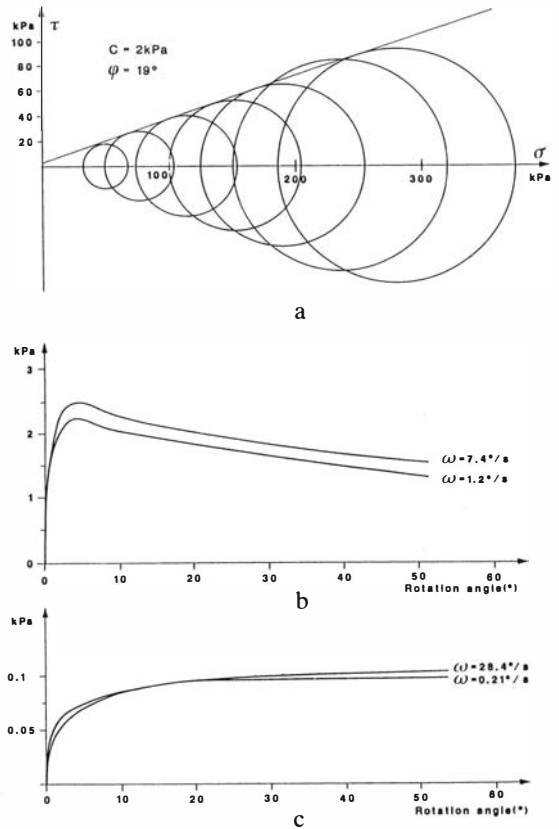


Fig. 5. Rheological tests on analog materials.

a. Triaxial tests on material 1 show Coulomb behavior with low friction angle of 19° .

b. Vane tests on material 1 show strain softening behavior and cohesion of 2 to 2.5 kPa.

c. Vane tests on material 2 show nearly perfectly plastic behavior with constant flow stress of about 100 Pa over two orders of magnitude in strain rate.

g/kg of silicone oil. As with any saturated clay, vane tests have shown a nearly perfectly plastic behavior with a low yield stress of 100 Pa which is constant over two orders of magnitude in strain rate (Fig. 5c).

Dynamic scaling

It is clear that a single layer of Coulomb material has a strength profile with depth which differs drastically from those inferred for continental lithosphere (Fig. 6). The main difference is that layers of high strength are observed in the lower crust and the uppermost mantle of continental lithosphere whereas in the Coulomb material layer, the lowermost part is the only and most resistant one. Nevertheless, it is possible to compare such a single layer

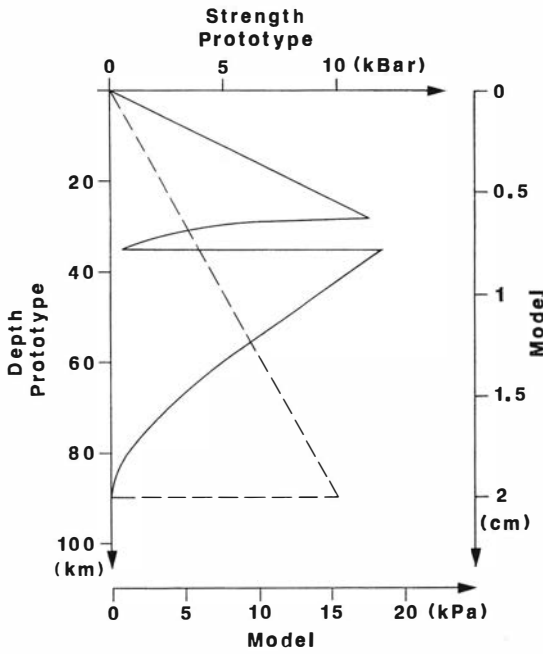


Fig. 6. Strength profile of continental lithosphere (full line, from Molnar and Tapponnier, 1981) compared with that of a single layer of Coulomb material (dashed line). Although the strength distribution at depth is different between prototype and model, the model is scaled with respect to gravity stresses in terms of depth-average strength (see text).

model with the continental lithosphere in terms of depth-averaged strength. Neglecting inertial terms, the equilibrium equation of a medium of density ρ under a gravity field g is:

$$\frac{\delta \sigma_{ij}}{\delta x_j} + \rho \cdot g_i = 0 \tag{1}$$

where σ_{ij} , x_j and g_i are respectively the components of the stress tensor, the space variable and the gravity field. If σ_c , h_c , ρ_c and g_c are characteristic quantities corresponding to the variables above, the non-dimensionalized form of equation (1) is:

$$\left(\frac{\sigma_c}{\rho_c \cdot g_c \cdot h_c} \right) \cdot \left(\frac{\delta \sigma'_{ij}}{\delta x'_j} \right) + \rho' \cdot g'_i = 0 \tag{2}$$

where primes indicate dimensionless quantities. The dimensionless force ratio $F_t/F_g = (\sigma_c/\rho_c \cdot g_c \cdot h_c)$ in equation (2) expresses the balance between tectonic forces and gravity induced forces. If the value of this ratio is the same in nature as in the experiment, the

model will be scaled with respect to gravity. If we now choose σ_c to be the average strength of the lithosphere and h_c its whole thickness, the following values

$$\begin{aligned} \sigma_c &= 5 \cdot 10^5 \text{ kPa,} \\ h_c &= 10^5 \text{ m,} \\ \rho_c &= 2.8 \text{ g/cm}^3, \\ \text{and } g_c &= 9.8 \text{ m/s}^2 \end{aligned}$$

with
and

give $F_t/F_g = 0.17$ for continental lithosphere. On the other hand, in our model:

$$\frac{F_t}{F_g} = \left(\frac{C}{\rho_c \cdot g_c \cdot h_c} \right) + \frac{1}{2} \tan(\phi) \tag{3}$$

where C and ϕ are the cohesion and the friction angle of the material. This ratio decreases and tends to $\frac{1}{2} \tan(\phi)$ as either ρ_c , g_c or h_c increases. Figure 7 shows variations of the ratio F_t/F_g with respect to the centrifuge acceleration for $h_c = 1, 2$ and 3 cm, $\rho_c = 2.8 \text{ g/cm}^3$, $C = 2 \text{ kPa}$ and $\phi = 19^\circ$. The asymptotic value is $\frac{1}{2} \tan(\phi) = 0.17$. It is clear from these curves that increasing centrifugal acceleration above about $80 g$ does not change significantly the value of the ratio F_t/F_g . We have thus chosen the value of $80 g$ and a model thickness of 2 cm to perform the experiments. The corresponding value of the ratio F_t/F_g is 0.22 and is of the same order of magnitude as the value of 0.17 calculated for a real continent.

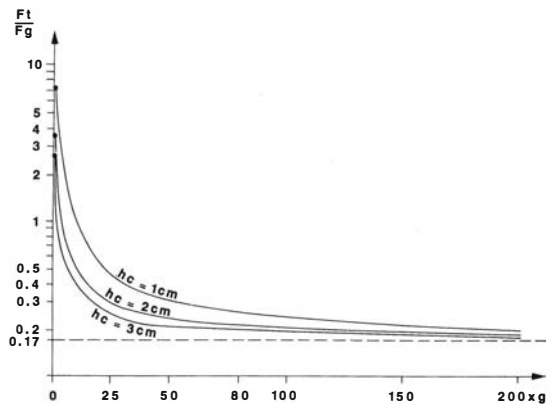


Fig. 7. Dimensionless force ratio F_t/F_g (in model case) of depth-averaged strength over characteristic gravity stress $\rho_c \cdot g_c \cdot h_c$ plotted against centrifuge acceleration (g_c) for density $\rho_c = 2.8 \text{ g/cm}^3$ and characteristic vertical length $h_c = 1, 2$ and 3 cm. Dots are values of this ratio under natural gravity. Note that increasing acceleration over about $80 g$ implies negligible variations of the force ratio near the asymptotic value of 0.17 .

3-D indentation experiment

Evolution of horizontal deformation pattern, comparison with the 2-D case

Figures 8a, b and c show three intermediate stages of the experiment taken by the remote camera fixed in the arm of the centrifuge. From that point of view, the upper quarter of the model is hidden by a part of the structure of the arm. The full view of the model in the final state is shown on Figure 9a. Low-angled lighting from the right-hand side emphasized the surface topography of the model. The photographs show that horizontal deformations occur principally along strike-slip faults which appear to absorb a large fraction of the total shortening. Evolution of the strike-slip fault pattern appears to follow rules similar to those in the 2-D plasticine case. After the formation of a "frontal triangle" bounded by two conjugate faults, alternatively right-lateral and left-lateral faults form and propagate into the medium. Because of the symmetric boundary conditions prevailing at the onset of the experiment, (unconfined on both lateral sides, see earlier), deformation begins by a symmetric pattern in which right-lateral and left-lateral faults play balancing roles (Fig. 8a, and b). During the first half of the experiment (between 3.5 cm and 9 cm of the indenter advance), most of the shortening is taken up by a right-lateral fault (F_2) which propagates towards the left-hand edge of the model, producing the lateral extrusion of a block to the left (Fig. 9b). This process stops as the extruded block comes into contact with the wall of the container. Then the experiment becomes asymmetric: successively, two large left-lateral faults (F_3 and F_4) propagate towards the right-hand side free edge of the model, producing the extrusion of two blocks to the right (Figs. 8b, c and 9a). This pattern of deformation resembles that observed in the 2-D case (figures 2c and d). More interesting however, are the differences which we interpret as being mainly due to the greater friction angle ($\phi=19^\circ$) in material 1 than in plasticine ($\phi\approx 0^\circ$, conjugate faults cross at about right angles). The 19° friction angle produces a departure from purely plastic, isovolumetric strain and makes the angle between the maximum principal horizontal stress and the faults smaller (35°). This more acute angle forces the faults to propagate farther (North) into the model before reaching the free edge, thus making the pie shaped faulted blocks of material 1 more elongated in that direction (N-S). This in turn has consequences on the extrusion kinematics of blocks. Roughly, in plane-strain, the velocity of lateral extrusion of a block is proportional to the cosine of the angle between the fault responsible

for the extrusion and the indenter front. Increasing the friction angle from purely plastic behaviour ($\phi=0^\circ$) increases that angle and thus reduces the amount of lateral extrusion and rotation of the block (Fig. 9a). This probably also partially accounts for the fact that right-lateral slip at the front of the indenter does not always occur, or is smaller than in the plasticine experiments (Fig. 2). Here, only a small right-lateral component of slip is visible on the thrust fault running parallel to the indenter, and deformation of the 2 cm grid in the triangular zone demonstrates more distributed dextral shear parallel to the indenter front (Fig. 9a). Thus, by contrast with the plasticine experiments, the eastward lateral extrusion of blocks appears to be controlled here by combined right-lateral slip on the right-hand side of the frontal triangle (F_2) and left-lateral slip on F_1 , F_3 , then F_4 (Fig. 9b).

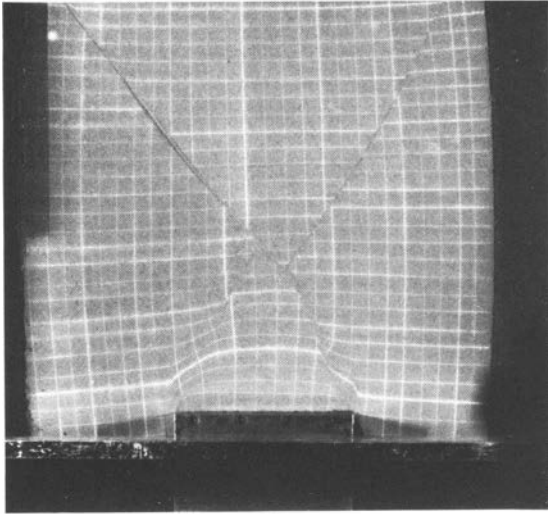
Final state: thickening, plane-strain, rifting

Though deformation involving vertical strain is difficult to see on Figure 8 a, b and c, the low-angled lighting on the photos of Figures 9 a, c and d emphasizes the zones where thickening or thinning of the model has occurred in the final state.

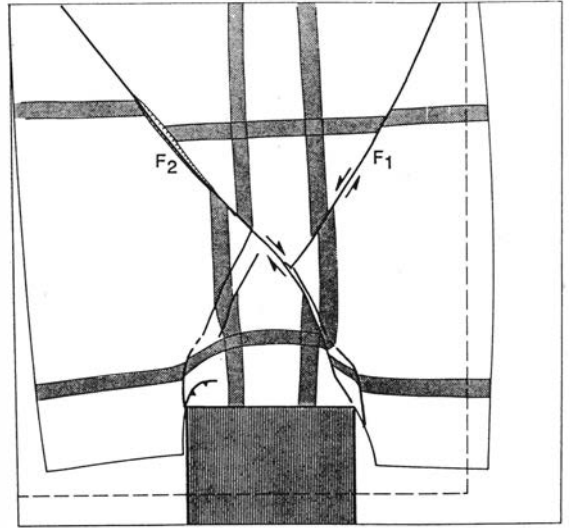
Thickening:

It is clear on Figure 9a that thickening is mostly localized in a double tipped triangular zone in front of the indenter, bounded by faults F_3 and F_2 , and F_4 and F_2 (Fig. 9b). Outside this domain, narrow zones of thickening occur locally along segments of strike-slip faults where the local curvature increases (e.g. on F_3 and F_4 , Fig. 9a and b). Segments of faults bounding the uplifted triangle have multiple splays on which thrusts, strike-slip, or oblique movements occur. For example, on the segment of F_2 which borders the triangle to the right, three or four distinct, roughly parallel splays can be seen. Thrust movements appear to have occurred principally on the most external splay where the steepest and highest topographic step is observed (Fig. 9c).

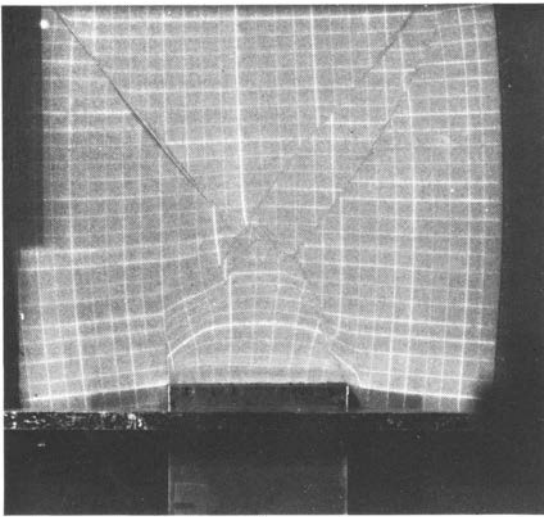
Within the triangle, the distortion of the 2 cm square grid indicates more diffuse deformation which may be accommodated by a large number of small indistinct faults (Figs. 9a and c). The decrease of surface area recorded by the initially square grid elements in this zone is 30–50 % and corresponds to a local thickening of the layer by 43–100 %. Direct measurements made on N-S sections of slices of the model, extracted from this zone at the end of the experiment, corroborate this inference. The



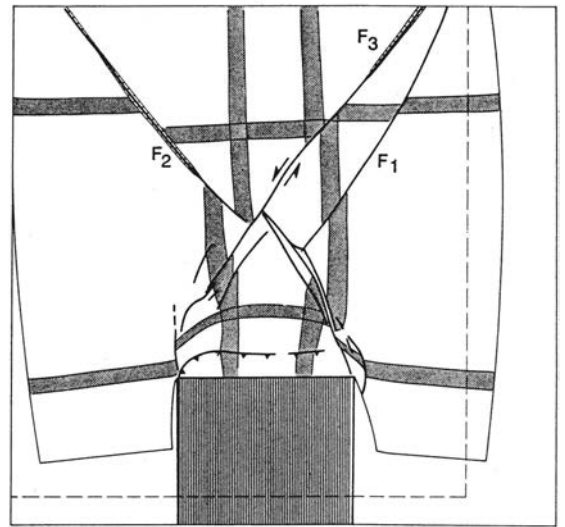
a



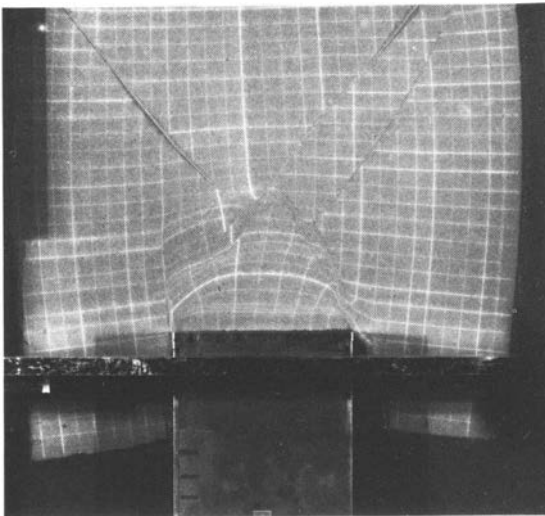
d



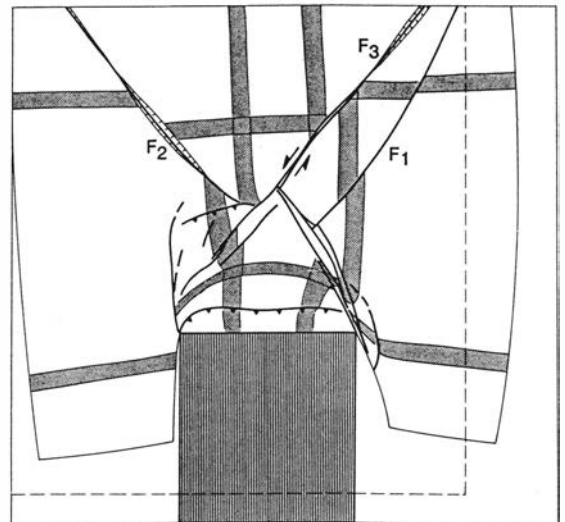
b

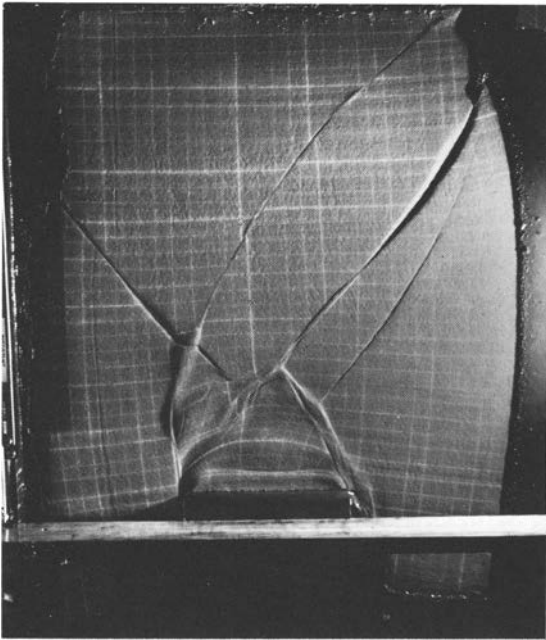


e

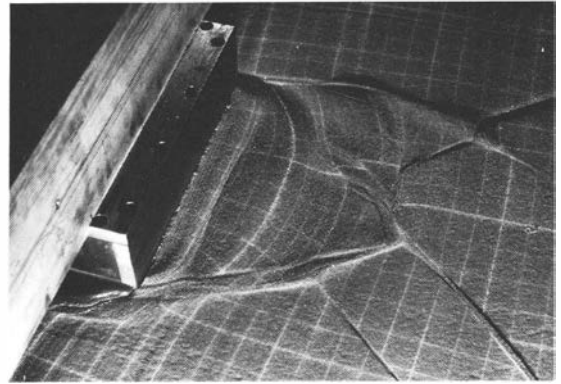


c

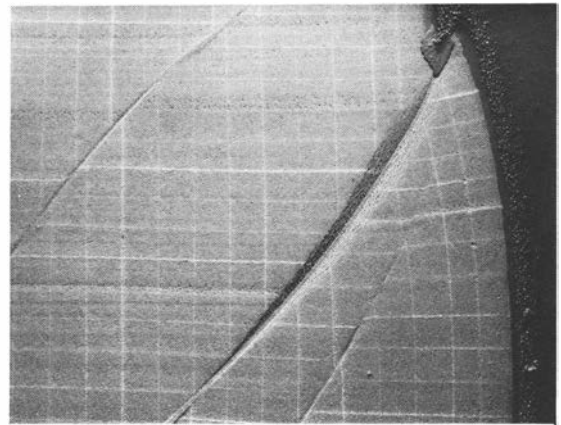




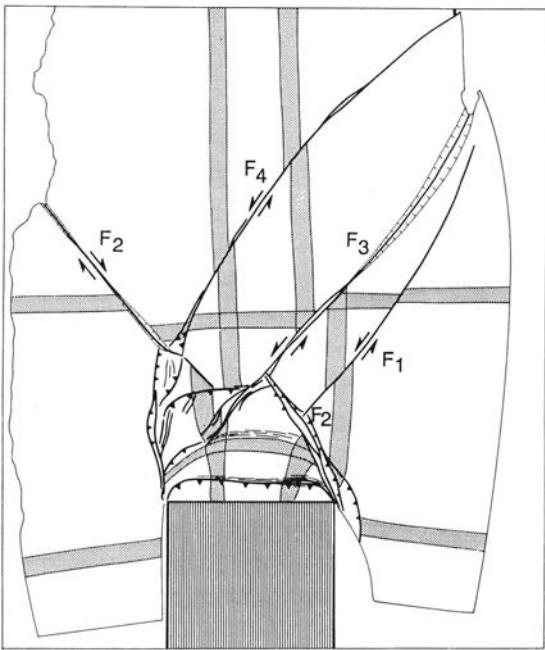
a



c



d



b

Fig. 9. a. Final state of experiment with low incident lighting emphasizing surface topography of model. Total displacement of the indenter is 20.8 cm. Thickening appears to occur only in the triangular frontal zone and along curved segments of strike-slip faults. Note the large rift along the major left-lateral fault on right-hand side of model.

b. Schematic interpretation of Figure 9a. Symbols are the same as in Figure 8d.

c. Detailed view of thickened zone in front of the indenter. Faults bounding frontal triangle appear to splay at the surface and bear strike-slip as well as thrust component of slip.

d. Detailed view of V-shaped rift along F_3 . Narrow strike-slip furrow is clear in the center of the rift. In rift deformations involve small en échelon cracks or normal faults trending parallel to free edge of model, i.e. perpendicular to least horizontal stress direction.

Fig. 8. a, b and c. Photos of three intermediate stages of indentation experiment taken during the rotation of the centrifuge. Note that upper part of model cannot be viewed from camera location. Flood-lighting flattens relief impression. Horizontal distortions of 2×2 cm grid show narrow shear zones or faults involving important strike-slip displacements. General fault pattern (in map view) resembles that of plane strain experiments (see Fig. 2). Indenter displacement for (a) is 9.4 cm; (b), 13.75 cm; (c), 18.75 cm.

d, e and f. Fault patterns drawn from Figure 8a, b and c. Dotted line indicates initial border of model. Shaded thick lines have been drawn from the 2×2 cm grid in order to emphasise horizontal displacements on faults. Hatched lines indicate rifts occurring along parts of strike-slip faults.

layer of material 1 increased in thickness by a factor of up to 2 in the most deformed parts. The fact that deformation appears to be rather homogeneous in the area where thickening occurs may be partly due to a local increase of the strength of the layer concurrent with thickening; this forces subsequent thickening to migrate towards adjacent zones of lesser thickness. Such a migration process is probably enhanced by the linear depth-dependence of strength in Coulomb materials which makes the total strength of the layer vary like the square of its total thickness (i.e. an increase of 10 % in thickness would imply an increase of 20 % of the total strength). The increase in potential energy induced by gravity forces in thickened zones also contributes to the migration of the deformation towards adjacent, unthickened parts. Simple calculations for mountain ranges have shown that, for a given amount of shortening, more work (against gravity) has to be done to increase the height of the range than to widen it (Molnar and Lyon-Caen, in press).

In addition to diffuse thickening, there is one large thrust parallel to the indenter (Figs. 9a, b and c). This thrust, located in the vicinity of the rigid indenter and parallel to it, may merge with its vertical front at the base of the model. Its "northward" vergence probably results from the fact that a vertical indenter front is poorly adapted to model underthrusting along a real collision front.

Overall however, the areal distribution and the steep limits of thickened zones in the experiment bear some similarities with the geographical extent, shapes and boundaries of regions thickened during Cenozoic times in Asia (Fig. 10). Although the question of where and when crustal thickening has taken place during the collision between India and Asia remains debatable, it has generally been assumed that most of it has occurred in regions where the present elevations are greater than 3 000 m (Fig. 10) (e.g. Molnar and Tapponnier, 1981). Thus, in a qualitative sense, comparison between Figures 9a and 10 might suggest the wide triangular zone in front of the indenter to represent Tibet and the narrower zone along the lower left-hand segment of F_4 to be similar to the Tien Shan range.

Rifting:

Figures 9a and d show that, away from the frontal zone, rifts formed in the experiment. They occur along large strike-slip faults (F_2 and F_3 , Figs. 9a and b) and are partly due to the lateral extrusion and small components of rotation of the blocks. Along F_2 , extrusion and rifting ceased as the extruded block came into contact with the wall of the container. By contrast, the block extruded by slip along

F_3 was free to move to the right and a wider V-shaped rift opened there (Figs. 9a, b and d). This rift reached the free edge of the model and the gap opened by the offset of that edge was filled with an influx of material 2 (Fig. 9d). Similar rift-like features (open gaps) linked with strike-slip faults were observed in the plasticine experiments (Fig. 2). As in the plasticine experiments however, where the rift opened along F_3 is related to the general geometry of that fault. F_3 has a sinuous shape and left-lateral slip along it is accommodated by compression left of the inflexion point, as attested by the small elevation observed there, and by rifting right of that point. No rifts have formed along F_4 , where no such curvature inversion is observed. We interpret this to result from the proximity of the far side (Northern) of the model which influences the path followed by the fault. Rifting occurs in Asia under similar circumstances along the Altyn Tagh – Gansu – Haiyuan fault zone (Figs. 1 and 10). Where the fault zone bends to the SE, in Gansu province, compression occurs in the Qi Lian mountains. East of 110°E, by contrast, where its strike veers to a more EW direction, extensional tectonics become important in the Shanxi and Qin Ling mountains (Fig. 10), (Peltzer et al., 1985). More generally, extension and rifting are observed in Asia near the Eastern and Southeastern borders of the continent (Fig. 10). Rift systems in these regions are clearly linked with the large strike-slip faults induced by the collision (Fig. 1). According to the extrusion model proposed and discussed in Peltzer et al. (1982), Tapponnier et al. (1982), Tapponnier et al. (1986) and Peltzer and Tapponnier (in press), (Fig. 1), the wider extensional zone which would have been created by left-lateral slip on the Red River fault, is the South China Sea.

At a more detailed level in the experiment (Fig. 9d), one may note that deformation within the rift involves numerous en échelon cracks striking nearly parallel to the "free" lateral boundary of the model, as expected in the vicinity of that boundary, to which the least principal horizontal stress is perpendicular.

Discussion: thickening versus plane-horizontal-strain

One of the main aims of this study was to assess, what fractions of the total shortening would be accommodated by thickening and by lateral extrusion in a 3-D gravity scaled indentation experiment. One easy way to deduce this quantitatively from the 2 cm

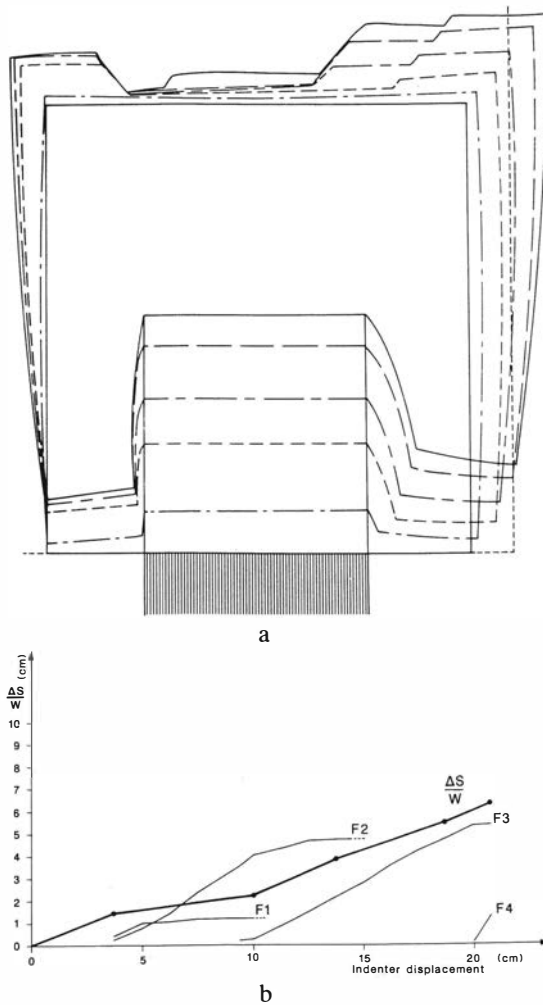


Fig. 11. a. Evolution of contour line deforming with model at different stages of experiment. No thickening occurs outside this contour. Dotted line indicates initial shape of model.

b. Thick line is the amount of indenter convergence accommodated by thickening in model plotted against indenter displacement. Points on curve are calculated from decrease of contour bounded areas of Figure 11a divided by indenter width W . Thin lines indicate progressive horizontal offsets on major faults, F_1 , F_2 , F_3 and F_4 .

square grid is to follow the deformation of a surface contour line including all the area where thickening has occurred (Fig. 11a). The surface area bounded by this line decreases as the thickness of the model increases. Assuming that deformation induces small volume changes, the decrease δS of this surface area at any stage is equal to the fraction of indenter penetration which has produced thickening, multiplied

by the width of the indenter (W). Figure 11b shows the variation of the quantity $\delta S/W$ as a function of increasing displacement of the indenter. Thickening appears to occur rather regularly during the experiment and to have absorbed, in the final stage, about 30 % of the total indenter displacement. At a more detailed level, however, between 3.5 cm and 10 cm of indenter penetration, the slope of the curve ($\delta S/W$) is smaller, by a factor of about 2, than for penetrations of less than 3.5 cm and more than 10 cm. This interval corresponds to the phase of fastest slip on F_2 (Figs. 8a and 11b) as attested by the large offset of the contour line of Figure 11a occurring between the second and third positions of the indenter on that figure. This decrease in the thickening rate may thus be accounted for by the fact that F_2 , a rather straight fault reaching the left-hand edge of the model, makes lateral extrusion an easier response to indenter penetration than thickening does at the same time. However, no such obvious decrease of the thickening rate is observed during extrusion phases in which F_3 and F_4 are particularly active (Fig. 11b).

In Asia, equivalent estimates cannot be made so easily. The major problems are the poor knowledge of the initial state of that continent before India collided with it, and the date of that collision. Although the displacement of India relative to Asia is relatively well constrained (Molnar and Tapponnier, 1975; Patriat et al., 1982), the positions and shapes of the continental margins of either India or Asia prior to the collision are quite uncertain. The age of the onset of the collision can only be indirectly estimated to be between 60 and 40 Ma. Thus, the total shortening Asia has undergone since that time is still very uncertain. Values of 2 000–3 000 km of intracontinental convergence between India and Asia since Eocene times however, do not contradict most of the published data (e.g. Jeager et al., 1982; Patriat et al., 1982; Besse et al., 1984). As discussed elsewhere (Tapponnier et al., 1986; Peltzer and Tapponnier, in press), rough estimates of combined offsets on the major faults allowing collision-induced extrusion of Sundaland (Wang Chao, Three Pagodas and Red River faults) and South China (Kunlun and Talytyn Tagh faults), may account for half of this total convergence. In any case, given the large uncertainties on all such numbers, the fraction of about 30 % of convergence taken up by thickening in the experiment is certainly compatible with the rough estimate of "less than 50 %" made by Tapponnier and others (1986), or the approximately 1 000 to 1 500 km of convergence estimated to have been absorbed in mountain building since the Eocene by Molnar and Tapponnier (1975).

Summary and conclusion

The centrifuge experiment presented in this paper marks a second step in laboratory experiments applied to large-scale continental tectonics. After a 2-D approach on plasticine models, we designed a two-layer model in which the upper layer (continental lithosphere) deforms in 3-D by localized shear as a result of strain-softening. In addition, an acceptable scaling with respect to gravity in terms of depth-averaged strength of the layer has been achieved by centrifuging at 80 g. The main results of this new study are:

- (1) As in the 2-D approach, indentation on unilaterally confined models produces lateral extrusion of blocks guided by large strike-slip faults.
- (2) Indentation also produces thickening, but much of it remains localized in a triangular zone bounded by conjugate strike-slip faults in front of the indenter. Thickening also occurs along strike-slip faults at places where the local curvature increases.
- (3) In the final stage, the fraction of shortening accommodated by thickening reaches about 30 %, the other 70 % being absorbed by lateral extrusion.
- (4) Rifts open along segments of strike-slip faults, near the free edge of the model.

Thus, although it adds a fundamental aspect lacking in previous analog experiments, this approach corroborates in many ways the results obtained in plane-horizontal-strain on plasticine models. The areal distribution of thickened zones and strike-slip fault-related rifts, respectively at the front of the indenter and near the free margin of the model, appears to be in good agreement with what we know of the Tertiary geology of Asia.

The major shortcoming of this new model is the rheology of the Coulomb material layer taken to be an analog of the continental lithosphere. Further experiments should involve more sophisticated multilayers in order to account better for the complex rheological depth profiles inferred for the continental lithosphere (e.g. Davy, 1987; Davy and Cobbold, 1987). Improving such experiments however, will be limited by the physical processes linked with variations of temperature during deformation which are essential in Nature but remain difficult to model in the laboratory.

Acknowledgements. — This study was supported by the Institut National des Sciences de l'Univers, ATP Grants 11–65 and 41–26. Numerous discussions with Paul Tapponnier were at the origin of this work. Special thanks go to J.F. Corté and J. Garnier from the Laboratoire Central des Ponts et Chaussées in Nantes for opening the centrifuge installation to geological research and for full assistance during the experiment. T.S. Luong and R. Barre

from the Laboratoire de Mécanique des Solides of the Ecole Polytechnique of Paris are thanked for contributing to rheological tests on analog materials, F. Delvert from the S.C.O.P. company for providing centrifuge-adapted camera equipment, and G. Avelin for drawing the figures. I also thank P. Tapponnier, Y. Gaudemer and R. Enkin for reading and improving the original manuscript, and C.K. Mawer and Ruud Weijermars for reviewing the last version. I.P.G.P. contribution n°966.

REFERENCES

- Besse J., V. Courtillot, J.P. Pozzi, M. Westphal, and Zhou Y.X. 1984: Paleomagnetic estimates of crustal shortening in the Himalayan thrusts and Zangbo suture, *Nature*, 311, 621–626.
- Caquot, A. and Kerisel, J. 1949: *Traité de Mécanique des Sols*, 2nd ed., Gauthiers-Villards, Paris, 385 p.
- Davy, P. 1987: The mechanism of crustal thickening versus the rheology of the lithosphere, abstract E.U.G., Strasbourg.
- Davy, P. and Cobbold, P. 1987: Experimental modelling of continental lithospheric deformation, abstract for Hans Ramberg Meeting, Uppsala, 22nd–24th April, 1987.
- England, P. and McKenzie, D. 1982: A thin viscous sheet model for the continental deformation, *Geophys. J. R. Astron. Soc.*, 70, 295–321.
- Jaeger, J.J., Adloff, C., Doubinger, J., Pons, D., Vozenin-Serra C. and Wang, N.W. 1982: The contribution of fossils to the Paleogeography of the Lhasa block (Tibet), *EOS*, 63, 1093.
- Molnar, P. and Lyon-Caen, H. in press. Some simple physical aspects of the support, structure and evolution of mountain belts, John Rogers Symposium, *Geol. Soc. Am. Mem.*
- Molnar, P. and Tapponnier, P. 1975: Cenozoic Tectonics of Asia: Effects of a continental collision, *Science*, 189, 419–426.
- Molnar P., and Tapponnier, P. 1981: A possible dependence of tectonic strength on the age of the crust in Asia, *Earth Planet. Sci. Lett.*, 52, 197–114.
- Patriat, P., Segoufin, J., Schlich, R., Goslin, J., Auzende, J.M., Beuzart, P., Bonnin, J. and Olivet, J.L. 1982: Les mouvements relatifs de l'Inde, de l'Afrique et de l'Eurasie, *Bull. Soc. Géol. France*, 24, 363–372.
- Peltzer, G. 1983: Naissance et évolution des décrochements lors d'une collision continentale; approche expérimentale, application à la tectonique de l'Est de l'Asie, Thèse de 3^{ème} cycle, University of Paris VII.
- Peltzer, G., Tapponnier, P. and Cobbold, P. 1982: Les grands décrochements de l'Est asiatique, évolution dans le temps et comparaison avec un modèle expérimental, *C.R. Acad. Sci.*, Paris, 294, 1341–1348.
- Peltzer, G., Gillet, P. and Tapponnier, P. 1984: Formation des failles dans un matériau modèle: la plasticine, *Bull. Soc. Géol. France*, 1, 161–168.
- Peltzer G., Tapponnier P., Zhang, Z.T. and Xu, Z.Q. 1985: Neogene and Quaternary faulting in and along the Qinling Shan, *Nature*, 317, 500–505.
- Peltzer, G. and Tapponnier, P., in press. Formation and evolution of strike-slip faults, rifts and basins during the India-Asia collision: an experimental approach, *J. Geophys. Res.*,
- Tapponnier, P. and Molnar, P. 1976: Slip-line field theory and large-scale continental tectonics, *Nature*, 264, 319–324.

- Tapponnier P. and Molnar, P. 1977: Active faulting and tectonics of China, *J. Geophys. Res.*, 82, 2905–2930.
- Tapponnier P., Peltzer, G., Le Dain, A.Y., Armijo, R. and Cobbold, P. 1982: Propagating extrusion tectonics in Asia: New insights from simple experiments with plasticine, *Geology*, 10, 611–616.
- Tapponnier P., Peltzer, G. and Armijo, R. 1986: On the mechanics of the collision between India and Asia, in *Collision Tectonics*, edited by J.G. Ramsay, M.P. Coward, and A. Ries, *Geol. Soc. London, Spec. pub.*, 19, 115–159.
- Villotote, J.P., Daignières, M. and Madariaga, R. 1982: Numerical modelling of intraplate deformation: simple mechanical models of continental collision, *J. Geophys. Res.*, 87, 10709–728.